

Preventing painful age-related bone fractures: Anti-sclerostin therapy builds cortical bone and increases the proliferation of osteogenic cells in the periosteum of the geriatric mouse femur

Michelle L Thompson, PhD¹, Stephane R Chartier, BS¹, Stefanie A Mitchell, BS¹ and Patrick W Mantyh, PhD^{1,2}

Abstract

Age-related bone fractures are usually painful and have highly negative effects on a geriatric patient's functional status, quality of life, and survival. Currently, there are few analgesic therapies that fully control bone fracture pain in the elderly without significant unwanted side effects. However, another way of controlling age-related fracture pain would be to preemptively administer an osteo-anabolic agent to geriatric patients with high risk of fracture, so as to build new cortical bone and prevent the fracture from occurring. A major question, however, is whether an osteo-anabolic agent can stimulate the proliferation of osteogenic cells and build significant amounts of new cortical bone in light of the decreased number and responsiveness of osteogenic cells in aging bone. To explore this question, geriatric and young mice, 20 and 4 months old, respectively, received either vehicle or a monoclonal antibody that sequesters sclerostin (anti-sclerostin) for 28 days. From days 21 to 28, animals also received sustained administration of the thymidine analog, bromodeoxyuridine (BrdU), which labels the DNA of dividing cells. Animals were then euthanized at day 28 and the femurs were examined for cortical bone formation, bone mineral density, and newly borne BrdU+ cells in the periosteum which is a tissue that is pivotally involved in the formation of new cortical bone. In both the geriatric and young mice, anti-sclerostin induced a significant increase in the thickness of the cortical bone, bone mineral density, and the proliferation of newly borne BrdU+ cells in the periosteum. These results suggest that even in geriatric animals, anti-sclerostin therapy can build new cortical bone and increase the proliferation of osteogenic cells and thus reduce the likelihood of painful age-related bone fractures.

Keywords

Aging, bone fracture, functional status, quality of life, morbidity, mortality

Date received: 29 August 2016; accepted: 3 October 2016

Introduction

In humans, peak skeletal mass and strength is reached when an individual is 25–30 years old and declines thereafter.^{1,2} By the time an individual reaches 60 years of age, osteoporosis, fragility fractures, and delayed fracture healing, which involve declines in the mass, strength, and healing properties of bone, become highly prevalent disorders.³ This aging-related bone loss predisposes individuals to an increased risk of bone fracture so that 50% of women and 25% of men over 60 years of age will suffer age-related fractures during their remaining lifetime.^{4–7} Age-related bone fractures usually heal slower

than bone fractures in the young⁸ and are frequently accompanied by chronic skeletal pain, loss of functional status, and increased morbidity/mortality.^{8,9}

¹Department of Pharmacology, University of Arizona, Tucson, AZ, USA

²Department of Pharmacology (Cancer Center), University of Arizona, Tucson, AZ, USA

Corresponding author:

Patrick W Mantyh, Department of Pharmacology, University of Arizona, 1501 North Campbell Avenue, Tucson, AZ 85716, USA.
Email: pmantyh@email.arizona.edu



A major reason why the treatment of age-related bone fractures remains so problematic is that relatively little is known about the mechanisms that drive fracture pain^{10,11} and why aging bone fractures take longer to heal.^{8,11} Currently, the two major classes of analgesics used to manage age-related bone fracture pain are NSAIDs and opiates.^{10,12} While NSAIDs can be effective in attenuating mild to moderate skeletal pain, sustained use of NSAIDs frequently results in significant unwanted gastrointestinal, hepatic, or renal toxicity.¹² Even more problematic is that NSAIDs have been shown to inhibit bone healing as prostaglandins play a role in bone formation.^{13–15} Opiates are also frequently used to treat fracture pain, but in the elderly, opiates frequently induce dizziness, vertigo, and cognitive clouding, which can result in further falls resulting in new bone fractures or re-injury of the operated bone or joint.¹⁶

While developing novel analgesics to treat bone fracture pain is one avenue to increase the functional status of patients with bone fractures, another avenue would be to administer novel osteo-anabolic agents to individuals at high risk for fractures and reduce the likelihood of the occurrence of the bone fracture.^{10,17} However, a major unanswered question is whether osteo-anabolic agents can stimulate the proliferation of osteogenic cells and build significant amounts of new cortical bone in light of the marked decrease in both the number and responsiveness of osteogenic cells in geriatric bone.^{8,18–20}

In this article, we address this question by focusing on geriatric mice, cortical bone, and a monoclonal antibody directed at the protein sclerostin (anti-sclerostin) which has previously been shown to build new bone in young and adult rodents, primates, and humans.^{21–29} Using this approach, we demonstrate that administration of anti-sclerostin in geriatric and young mice markedly builds significant amounts of new cortical bone, increases bone mineral density, and significantly increases the proliferation of osteogenic cells in the periosteum. These data suggest that anti-sclerostin therapy may be an effective strategy to reduce the incidence of painful age-related bone fracture even in very old bone.

Materials and methods

Animals

Experiments were performed on 84 adult male C57BL/6J mice. Each experimental group contained an “n” that was equal to or greater than five. Animals were obtained from Jackson Laboratories, Bar Harbor, ME, and the animals were 4 (young) and 20 (geriatric) months of age at the start of the experiments and weighed 30 to 40 g. The mice were housed in accordance with the National Institutes of Health guidelines under specific pathogen-free conditions in autoclaved cages maintained at 22°C

with a 12-h alternating light/dark cycle and access to food and water *ad libitum*. All procedures adhered to the guidelines of the Committee for Research and Ethical Issues of the International Association for the Study of Pain and were approved by the Institutional Animal Care and Use Committee at the University of Arizona (Tucson, AZ) (Protocol Number: 08–005).

Anti-sclerostin treatment

After pilot experiments were performed to assess periosteal cell labeling produced by the bromodeoxyuridine (BrdU)-loaded osmotic pumps, the young and geriatric animals were randomly divided into two treatment groups: (1) naïve mice that received vehicle (PBS) treatment for a period of 28 days; and (2) naïve mice that received anti-sclerostin (25 mg/kg) treatment for a period of 28 days. Beginning on day 0 and every five days thereafter, animals were administered either vehicle or anti-sclerostin by intra-peritoneal (i.p.) injection. The anti-sclerostin sequestering antibody was kindly provided by Drs. Kris Poulsen and David Shelton (Rinat/Pfizer, San Francisco, CA) and the dose of anti-sclerostin used was similar to that used in previous studies.^{21–29}

5-Bromo-2'-deoxyuridine (BrdU) administration

BrdU is a synthetic nucleoside that is an analog of thymidine. BrdU is incorporated into the newly synthesized DNA during the S phase of the cell cycle, substituting BrdU for thymidine during DNA replication. In order to visualize proliferating cells in the periosteum under normal conditions, mice were placed under isoflurane anesthesia and implanted subcutaneously (s.c) with a single mini-osmotic pump (Alzet; Model 1007D) containing BrdU (Sigma-Aldrich, B5002; St. Louis, MO) at a final concentration of 10 mg/ml (dissolved in sterile 1× Dulbecco's phosphate-buffered saline [DPBS]) (Mediatech, Inc., 21-031-CV; Manassas, VA). The pump was loaded with BrdU solution per manufacturer's instructions. The pump releases 0.5 µL of solution per hour for seven consecutive days (day 21–28) allowing for consistent and reproducible BrdU staining.^{30–35}

Measure of bone formation

Radiology. High-resolution radiograph images of naïve femurs were obtained at day 0 before injection of vehicle (PBS) or therapy (anti-sclerostin) to establish a baseline using the Faxitron MX-20 DC12 digital cabinet X-ray system (Faxitron, Tucson, AZ). Radiographs were then acquired every seven days until the experiment was complete. Mice were lightly anesthetized subcutaneously with ketamine/xylazine (0.005 mL/g, 50/5 mg/kg, respectively; Western Medical, 121127A; Arcadia, CA;

Sigma-Aldrich, 534056) to enable consistent placement of the animal for radiologic assessment. Faxitron settings were optimized for radiological assessment of cortical thickness. The settings used were 12-s exposure, 30 kV, center (4325), width (8456), and 4× and 8× magnification. Images were saved as dicom and TIFF files after a sharp setting of 2 was applied to each radiograph. Images were cropped in Adobe Photoshop (Adobe Systems Inc., San Jose, CA).

Distal cortical thickness. Images (TIFF) of vehicle- and anti-sclerostin-treated animals from days 0 and 28 were opened in Image J (NIH). Three measurements using the “straight” tool were taken from the medial and lateral aspects of the distal mid-diaphysis cortical bone. The medial and lateral measurements were added together and the three total measurements were averaged together. To determine the percent change of distal cortical thickness from day 0 to day 28, the following calculation was performed: $(\text{Day 28} - \text{Day 0}/\text{Day 0}) \times 100$. Data are presented for young (4 months old) and geriatric (20 months old), vehicle- and anti-sclerostin-treated animals.

Bone mineral density. Bone property measurements were conducted with the PIXImus dual-energy X-ray densitometer (General Electric Medical Systems, Milwaukee, WI). Calibration of the instrument was conducted as recommended by the manufacturer. One excised femur from each mouse was used to measure bone mineral density (BMD). All the bones were analyzed in the same orientation on the scan window and performed by the same person blinded to the age and conditions. BMD is presented as mg/cm^2 .

Preparation of tissue for immunohistochemistry and histology

At the completion of therapy administration at day 28, mice were deeply anesthetized with ketamine/xylazine (0.01 ml/g, 100/10 mg/kg, s.c.) and perfused intracardially as previously described.³⁶ Femurs were decalcified and processed for histology or immunohistochemistry as previously described.³⁶ Tissue was cut serially at either 10 or 20 μm sections and thaw mounted with two sections of bone per gelatin-coated slide. The 10- μm -thick sections were used for histology and stained with hematoxylin and eosin and the 20- μm -thick sections were used for immunohistochemical staining.

To enhance the staining and visualization of BrdU, an antigen retrieval protocol was used in combination with our normal immunohistochemical protocol. In order to perform immunofluorescent staining, the slides were dried at room temperature (RT) for 30 min and washed in 0.1 M PBS three times for 10 min each (3 \times 10). Next,

the slides were incubated at 37°C with 2 M HCl for 30 min and then washed with borate buffer (pH 8.5; BupH Borate Buffer Packs, Cat#28384, ThermoFisher Scientific, Grand Island, NY, USA) for 5 min. Slides were then washed in PBS for 3 \times 10 min. Next, the slides were blocked with 3% normal donkey serum (Jackson ImmunoResearch, Cat# 017-11-121; West Grove, PA) in PBS with 0.3% Triton-X 100 (Sigma Chemical Co., Cat# X100; St. Louis, MO, USA) for 1 h. Afterwards, the slides were incubated overnight with primary antibodies made in 1% normal donkey serum and 0.1% Triton-X 100 in 0.1 M PBS at RT. Proliferating cells were stained with BrdU (sheep anti-mouse; 1:300; Cat# B2850-01; US Biologicals, Salem, MA, USA).

After primary antibody incubation, preparations were washed 3 \times 10 min each in PBS and incubated for 3 h at RT with the secondary antibody conjugated to fluorescent Cy2 (1:100, anti-sheep; Cat# 713-226-147; Jackson ImmunoResearch). Preparations were then washed 3 \times 10 min each in PBS. Cellular nuclei were labeled using 4',6-diamidino-2-phenylindole (DAPI) (1:500; Cat#D21490; Invitrogen, Grand Island, NY) followed by an additional 3 \times 10 min wash in PBS. Slides were dehydrated through an alcohol gradient (2 min each; 70%, 80%, 90%, and 100%), cleared in xylene (2 \times 2 min), and cover slipped with di-n-butylphthalate-polystyrene-xylene (Sigma Chemical Co., Cat#06522). Preparations were allowed to dry covered at RT for 12 h before imaging.

Bright field and laser confocal microscopy

Bright field images of histologically stained sections were acquired using an Olympus BX51 microscope fitted with an Olympus DP70 digital CCD camera and an UPlanSApo 10 \times /0.40 objective. Confocal images of BrdU and DAPI were acquired using an Olympus FV1200 microscope (Olympus Life Sciences, Center Valley, PA) and a 60 \times /1.42 PlanApo N objective using excitation beams 488 and 405 and detected using BA505–540 and BA430–470 emission filters, respectively. Sequential acquisition mode was used to reduce bleed-through from fluorophores. The average volume of collected data was 211.7 $\mu\text{m} \times 211.7 \mu\text{m} \times 25 \mu\text{m}$, with each Z-axis slice being 0.5 $\mu\text{m}/\text{slice}$.

Cambium layer thickness

In order to measure the thickness of the cambium layer, images (TIFF) acquired under the DAPI channel of vehicle (PBS)- and therapy (anti-sclerostin)-treated animals from days 0 and 28 were opened in Image J (NIH). Three measurements using the “straight” tool, perpendicular to the cortical wall, were taken of the cambium layer of the

periosteum located approximately 4 mm from the distal end of the femur. The three total measurements were averaged together and data were presented in thickness (μm) of the cambium layer of the periosteum.

Quantifications

In order to quantify the number of proliferating cells in the periosteum, 20- μm -thick frozen sections were used, as cross-sectional analysis allowed for the visualization of the bone's anatomy (e.g. the condyles and growth plate), which enabled the observer to locate the same anatomical area when quantifying different animals. For each animal analyzed, at least three images were obtained of the distal diaphyseal periosteum (the distal region was defined as the periosteal area approximately 4 mm from the distal femoral condyles) and images were acquired at least 100 μm apart (i.e. five sections) to minimize duplication of quantifications.

Cell proliferation. Cellular proliferation was measured as the percentage of DAPI+ nuclei in each periosteal layer that are marked with BrdU. This endpoint was quantified in the following way: Olympus Image Binary files were obtained with the FV1200 microscope and saved as 16-bit files, then converted to TIFF files and opened with ImageJ (NIH) software. The total number of DAPI+ cells was manually tallied. Next, the corresponding image of BrdU+ was overlaid with the DAPI image in order to count the number of DAPI+/BrdU+ cells. The percentage was calculated by entering the total number of DAPI+ and DAPI+/BrdU+ into a Microsoft Excel worksheet. Inclusion criteria for BrdU+ nuclei were similar to those reported by Horner et al.³⁷ Specifically, BrdU immunostaining needed to be located in the nucleus as determined by counterstaining sections with DAPI and BrdU+ nuclei needed to exhibit uniform staining throughout the nucleus.

Bone-lining cells. The percentage of BrdU+ bone-lining cells was quantified in a similar way as described above. TIFF files were opened with ImageJ software and the total number of DAPI+ cells that were immediately adjacent to cortical bone was tallied. Next, the corresponding BrdU image was overlaid with the DAPI image and the number of BrdU+ cells immediately adjacent to cortical bone and that co-expressed DAPI were counted. The percentage was calculated by entering the total number of DAPI+ and DAPI+/BrdU+ into a Microsoft Excel worksheet.

Nuclear volume. In addition to the 2D analysis described above, cellular proliferation was visualized using a commercially available software program, Imaris—Surfaces

(Bitplane AG, South Windsor, CT). The Olympus Image Binary image files exported from the Olympus software were imported into Imaris and further analyzed for detailed quantitative and qualitative 3D characterization. The Imaris program tool, “Surfaces,” was used to generate a 3D solid mask (i.e. paint a surface over) of the original confocal signal. Previously published software parameters for volume rendering of the cells could not be found. The BrdU and DAPI confocal signal (i.e. voxels) was used to define the spatial location of the cellular nuclei. The only manual input made was to define the background threshold for all images as 2.000 μm ; all other parameters provided by the program were set automatically by the program to remove observer bias. The surfaces tool then applied a mask and created a 3D outline of the cellular nuclei. After volume rendering, the BrdU+ cells, immediately adjacent to the cortical bone or throughout the cambium layer, were manually selected and the volumes (given in μm^3) were tallied in Microsoft Excel. The average volume of a DAPI and/or BrdU+ throughout the cambium layer and at the bone-lining surface was calculated by taking the total nuclear volume and dividing that by the corresponding number of cells to get nuclear volume per cell. No further image processing was done on the images.

Statistical analysis

All statistical analyses were calculated in SigmaPlot software (San Jose, CA). One-way ANOVA was performed followed by a Tukey's post-hoc test comparing each group to each other at each age. Significance level was set at $p < 0.05$. In all cases, the investigator responsible for imaging and quantification was blind to the age and treatment of each animal.

Results

Administration of anti-sclerostin builds bone in young and geriatric mice

Naïve young (4 months old) and geriatric (20 months old) adult mice were administered either vehicle or anti-sclerostin for 28 days. Following 28 days administration of vehicle alone, the thickness of the cortical bone thickness had increased in the young adult animals and decreased in geriatric animals (Figure 1). In contrast, in both young (Figure 1(b) and (c)) and geriatric (Figure 1(d) and (e)) animals administered anti-sclerostin, there was a significant increase in the thickness of cortical bone (Figure 1(f)). Anti-sclerostin therapy also increased BMD in the distal head of the femur in both geriatric and young animals compared to administration of the vehicle alone (Figure 1(g)).

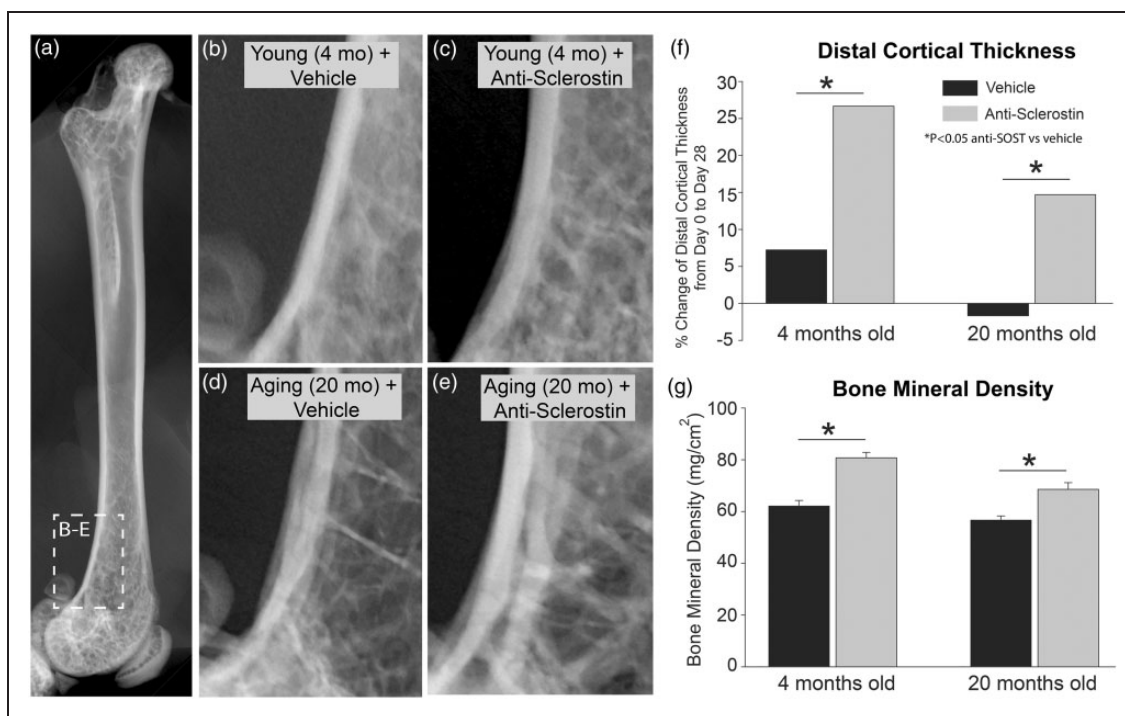


Figure 1. Anti-sclerostin increases the thickness of cortical bone and bone mineral density in young and geriatric mice. (a) Anterior/posterior (AP) radiograph of a naïve young (4 months old) male C57Bl/6 mouse shown for orientation. (b–d) Representative radiographs of the distal end of the femur of young (4 months old) (b, c) and aging (20 months old) (d, e) mice showing bone following of vehicle (b, d) or anti-sclerostin (25 mg/kg, i.p.) (c, e) for 28 days. (f) Histogram showing the percent change of thickness of the cortical bone in the distal head of the femur after 28 days of vehicle vs. anti-sclerostin treatment. Note that following 28 days administration of vehicle alone, the cortical thickness increased in young adult animals and decreased slightly in aging animals. In contrast, in both young and geriatric animals administered anti-sclerostin, there was a significant increase in the thickness of cortical bone. (g) Anti-sclerostin therapy also increased bone mineral density (BMD) in the distal head of the femur compared to administration of the vehicle alone. Bars represent mean \pm SEM; $p < 0.05$ after a one-way ANOVA, Tukey's post-hoc test.

Morphological characteristics of the layers of the periosteum

Periosteal tissue from the distal diaphysis of the femur from young and geriatric mice was used for this study (Figure 2). This region of the femur is highly cellular and best displays the cellular morphology throughout the two periosteal layers. The sparsely cellular fibrous layer is composed of loose fibrous tissue and spindle-shaped fibroblast-like cells. In contrast, the densely populated cambium layer is composed of more tightly packed cells with variable cell morphology: cuboidal and thin, spindle-shaped (Figures 2(c), (d)).

The cellularity and morphology of the two periosteal layers was confirmed using confocal microscopy and DAPI counterstaining (Figures 2(e) and (f)). In addition to reduced thickness, there is also a reduction in cell proliferation in the periosteum with age. This was determined after the animals had been exposed to BrdU through a mini-osmotic pump for seven consecutive

days. The majority of actively dividing cells was distributed throughout the cambium layer of the young and geriatric animals as very little BrdU+ cells were detected in the fibrous layer (Figures 2(e), (f)).

Administration of anti-sclerostin increases the proliferation of cells in the periosteum

To investigate whether anti-sclerostin could drive cell proliferation in the periosteum of geriatric and young animals, incorporation of BrdU (that was administered via osmopump from days 21–28) was examined in both geriatric and young mice that were receiving sustained administered anti-sclerostin from days 0 to 28. Animals receiving anti-sclerostin showed an increase in both cellular proliferation (Figure 3) and an increase in nuclear volume (Figure 4) when compared to animals that were receiving vehicle. Both geriatric and young animals receiving anti-sclerostin exhibited a significant increase in the number of BrdU+ cells in the cambium layer as

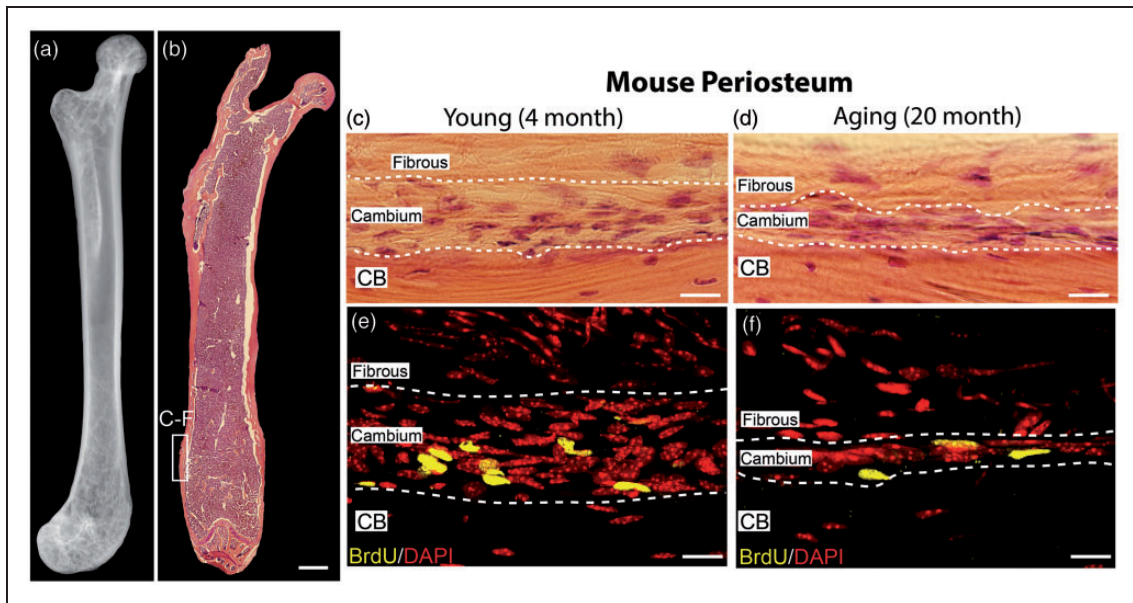


Figure 2. Anatomical localization of the mouse periosteum analyzed in the present study and the decline in the thickness, cellularity, and proliferation of cells in the cambium layer of the periosteum with aging. (a) Anterior/posterior (AP) view of a radiograph and (b) a representative low power of hematoxylin and eosin (H&E) image of the femur from a naïve young male C57Bl/6 mouse. The white-boxed region in the distal head of the femur show the location where histological and confocal images and measurements of cellular proliferation, nuclear volume, and cambium thickness were performed in this study. (c, d) Representative high-power H&E images of the naïve young (4 months old; c) and aging (20 months old; d) showing the cell-poor fibrous layer, the cell-rich cambium layer, and the underlying cortical bone. (e, f) Representative high-power confocal images showing that following administration of vehicle alone from 0 to 28 days, and BrdU from days 21 to 28, >90% of the BrdU+ cells were present in the cambium vs. the fibrous layer and there is a significant decline in BrdU+ cells in the cambium layer in the aging vs. young mice. To compare cell proliferation with age, BrdU was administered by mini-osmotic pumps for seven consecutive days and then stained for BrdU (yellow) and counterstained with DAPI (red). Note the decline in the thickness of the cambium layer and the number of BrdU+ cells in the geriatric (f) vs. young mice (e). Scale bar (a and b) 1 mm, (c–f) 20 μ m. CB: cortical bone.

compared to their respective vehicle counterparts. There was also a significant increase in the number of BrdU+ proliferative cells located at the bone-lining layer with anti-sclerostin treatment (Figures 3(b) and (d)). Finally, there was a notable increase in the nuclear volume of the proliferating cells (Figure 4).

In the young and geriatric mice, the effect of anti-sclerostin in the periosteum was also examined in terms of changes in cellular proliferation (as measured with BrdU+ cells), distribution of newly borne BrdU+ cells, the nuclear volume of newly borne BrdU+ cells, and the overall thickness of the cambium layer (Figure 5) following administration of vehicle vs. anti-sclerostin. In the young animals administered vehicle vs. anti-sclerostin, there was a significant increase in newly borne BrdU+ cells (11.7% vs. 23.8% of the total cells (all cells label with DAPI) (Figure 5(a)). In the geriatric animals, there was also a highly significant increase when comparing vehicle vs. anti-sclerostin (5.6% to 16.6%) in the number of newborn BrdU+ cells in the cambium layer (Figure 5(a)).

Anti-sclerostin also induced a marked increase in the number of newly borne cells in the bone-lining layer (which is where new cortical bone is formed) as

compared to animals that received vehicle alone. Thus, in vehicle-treated young animals, 16% of the bone-lining cells in the cambium layer of the periosteum were BrdU+ cells, whereas 37% of the cells were BrdU+ in the young animals that received anti-sclerostin therapy. Similarly, in the geriatric animals, there was nearly a 113% increase in the percent of BrdU+ cells at the bone-lining region (10.4% to 22.1%) with anti-sclerostin treatment (Figure 5(b)).

Previous reports have indicated that an increase in nuclear volume can be indicative of cells undergoing differentiation and/or an increase in cellular activity.^{38,39} The nuclear volume of BrdU+ and DAPI+ cells at the bone-lining layer of young and geriatric animals treated with anti-sclerostin was 65% and 72% larger, respectively, compared to vehicle-treated animals (Figure 5(c)). Interestingly, although anti-sclerostin induced an increase in cell proliferation, the number of newly born BrdU+ at the bone-lining layer, and the nuclear volume of newly borne cells, there was no significant change in the overall thickness of the cambium layer thickness when comparing vehicle- vs. anti-sclerostin-treated young or geriatric animals (Figure 5(d)).

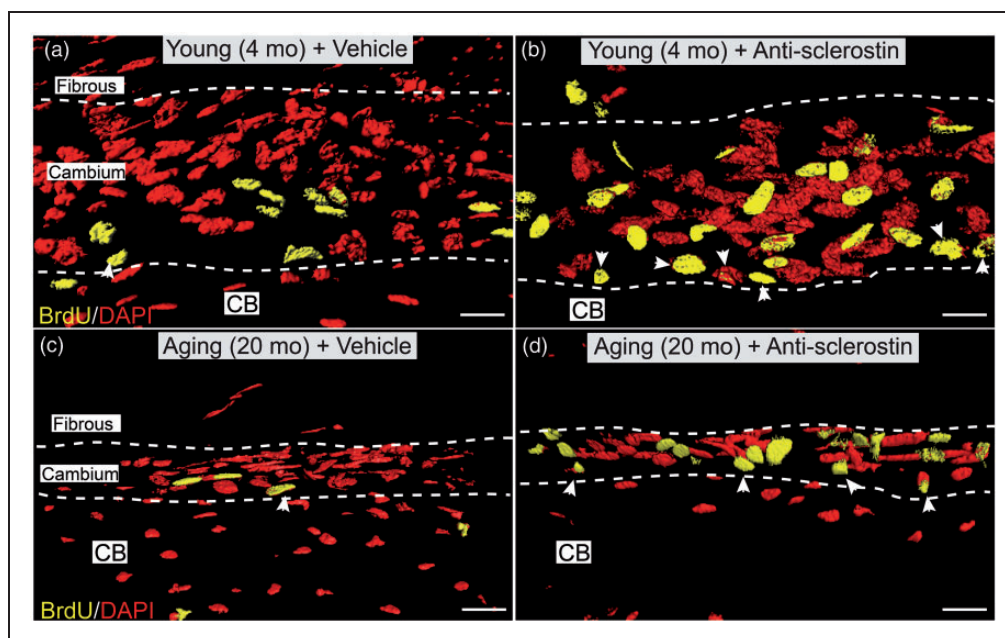


Figure 3. Confocal images showing that administration of anti-sclerostin increases the number of BrdU+ cells in the cellular “cambium” layer of the periosteum. (a–d) Representative high-power confocal images (3D-rendering performed with Imaris software) of decalcified frozen section of the cambium layer from distal mid-diaphysis of the femur from the young (4 months old) (a, b) and aging (20 months old) (c, d) animals administered vehicle (PBS) (a, c) or anti-sclerostin (25 mg/kg, i.p.) (b, d) every five days for 28 consecutive days. During the last seven days (days 21–28) animals were implanted with a mini-osmotic pump which provided continuous systemic release of BrdU. After decalcification and cutting frozen section of bone, sections stained with an antibody raised against BrdU (yellow; marker for cellular proliferation) and counterstained with DAPI (red; marker for nuclei). Note the increased number of BrdU+ cells in the cambium layer of anti-sclerostin (b, d) vs. vehicle (a, c) treated animals. Also note the increased number of BrdU+ cells at the interface between the cambium layer and cortical bone was termed the bone-lining layer (arrow heads). Scale bar, 30 μ m. CB: cortical bone.

Discussion

Age-related bone fractures, which are also known as “fragility fractures,” are unique in that they are most frequently caused by low-impact falls such as falling over a carpet or a pet, which would not result in a bone fracture in a young, healthy individual. Thus, in the young, the main etiology of a fracture is high-energy trauma. Fractures of the femoral neck, vertebrae, and distal radius following a fall or low energy trauma occur almost exclusively in the geriatric population and are a hallmark of osteoporosis.^{8,17} Importantly, these age-related bone fractures are frequently accompanied by chronic skeletal pain and an increase in morbidity and mortality. This is especially true of hip fractures (90% of “hip” fractures are actually a fracture of the proximal neck of the femur) as these almost invariably result in significant skeletal pain, loss of mobility, and hospitalization. Thus, 20% of individuals who are over 60 years with hip fractures die within a year of fracture, 20% will require nursing home care within a year of the fracture and will never return to living independently, and the great majority will never fully regain their pre-fracture gait, full functional status, and ability to walk long distances.^{8,9,12}

Here, we explore the effects anti-sclerostin had on increasing the thickness of cortical bone, as increasing cortical bone thickness is known to reduce the incidence of painful age-related fractures of the femur in the elderly.¹⁷ Sclerostin is a cysteine-knot glycoprotein that is a product of the *SOST* gene that is predominately expressed in bone by osteocytes and chondrocytes.^{40–42} Sclerostin was first identified in the study of two rare autosomal recessive disorders, sclerosteosis and van Buchem disease, which are associated with absent or reduced levels of sclerostin.^{43–45} Interestingly, although homozygote patients with these disorders have serious adverse clinical consequences due to excessive bone growth,⁴³ heterozygote patients have a normal phenotype, high bone mass, and very low risk of fractures.^{44–46} This has led to the concept that patients with low levels of sclerostin continually build bone throughout their life and that downregulation or sequestration of sclerostin in bone might be effective in promoting new bone formation.^{21–29} However, what is currently not clear, given the decreased thickness and number and responsiveness of osteogenic cells in aging periosteum, is whether anti-sclerostin can build new cortical bone and stimulate the proliferation of osteogenic cells in the geriatric periosteum.

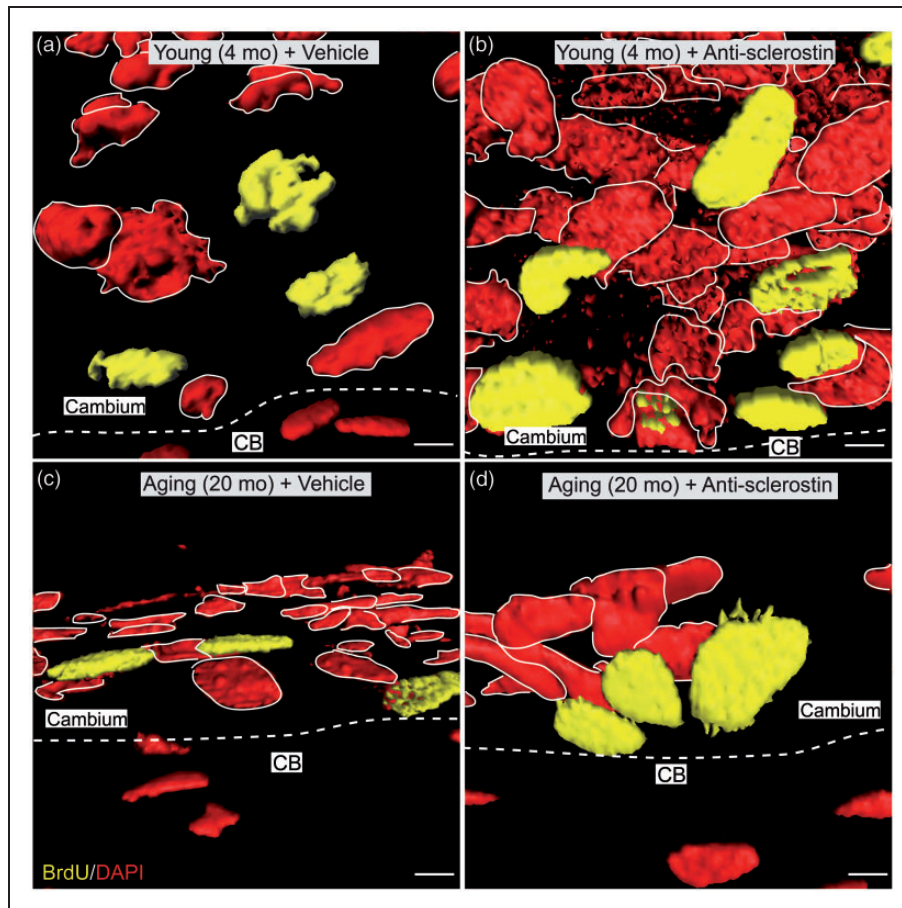


Figure 4. Confocal images showing that administration of anti-sclerostin increases the nuclear volume of both BrdU+, DAPI+ and BrdU-, DAPI+ cells in the bone-lining zone of the cambium layer of the periosteum. (a–d) Representative high-power confocal images (3D-rendered in Imaris software) of decalcified frozen sections of the cambium layer from young (4 months old) (a, b) and geriatric (20 months old) (c, d) where the interface between the cambium layer and cortical bone is delineated by a dashed, white line. Animals administered either vehicle (PBS) (a, c) or anti-sclerostin (25 mg/kg, i.p.) (b, d) every five days for 28 consecutive days. During the last seven days (days 21–28), all animals were implanted with a mini-osmotic pump that provided sustained release of BrdU. After tissue processing, sections were stained with BrdU (yellow; marker for cellular proliferation) and counterstained with DAPI (red; marker for nuclei). DAPI (red) is outlined in white to distinguish between each nucleus. Scale bar, 6 μ m. CB: cortical bone.

What was somewhat unexpected in the present study was just how robustly anti-sclerostin promoted an increase in cortical thickness in geriatric mice as previous studies have shown that there is a remarkable thinning of the cambium layer of the periosteum with aging so that the thickness of the cambium layer in a 2-year old rabbit is only 10% of that for a 14-day old rabbit.^{18,20,47} Importantly, the highly cellular cambium layer of the periosteum is where both stem and mesenchymal progenitor cells reside, and it has been argued that the periosteum is a key and often underappreciated tissue that can build new cortical bone in the elderly.^{11,17–19} In light of this dramatic thinning, a major question was whether this decrease in the number and division capacity of the stem and mesenchymal progenitor cells would also mean that the periosteum would no longer be responsive to signaling molecules that would drive

cortical bone formation.^{11,20} However, the present study suggests that even when given for a relatively short period (28 days) to geriatric animals, anti-sclerostin produced a significant increase in cortical bone thickness, bone mineral density, and the proliferation of osteogenic cells in the mouse periosteum.

In light of these observations, a major question is whether there are any therapies on the horizon that could potentially synergize with anti-sclerostin to increase cortical bone formation and reduce age-related skeletal pain so as to increase the mobility and functional status of geriatric patients. One therapy that might be synergistic with anti-sclerostin would be anti-nerve growth factor (anti-NGF). Previous studies have shown that anti-NGF reduces pain due to osteoarthritis as well as low back pain and both of these conditions are very common in the elderly.^{48–50} Importantly, anti-NGF

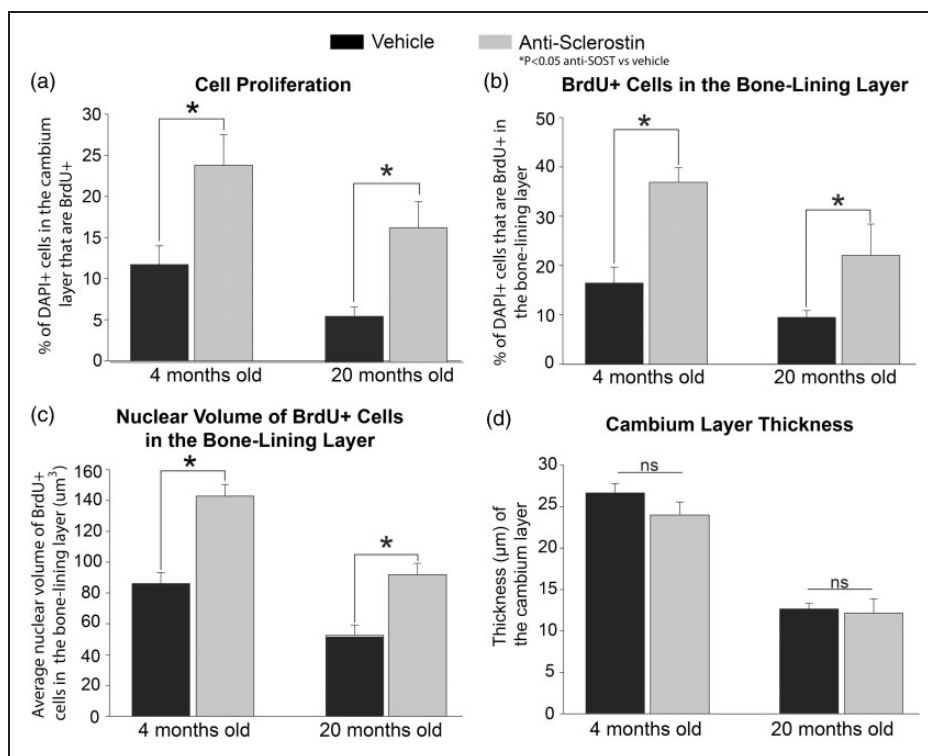


Figure 5. Histograms showing that administration of anti-sclerostin increases the proliferation of cells in the cambium layer of the periosteum. (a–d) Histograms illustrating the changes to the periosteum with administration of anti-sclerostin (25 mg/kg, i.p.; gray bars) or vehicle (PBS; black bars) every five days for 28 consecutive days to young (4 months old) and aging (20 months old) animals. (a) There is a significant increase in cell proliferation (percentage of DAPI cells marked with BrdU) in the cambium layer after administration of anti-sclerostin in both young and old animals compared to vehicle treated animals. (b) Anti-sclerostin-treated animals had an increase in the total number of DAPI+ cells that were BrdU+ cells at the bone-lining zone in both young and old animals compared to vehicle-treated animals. (c) Administration of anti-sclerostin increased nuclear volume of BrdU+ at the bone-lining surface in young and old animals compared to vehicle-treated animals. (D) Administration of anti-sclerostin has no effect on the cambium layer thickness compared to vehicle-treated animals in either age groups. Bars represent mean \pm SEM; $p < 0.05$ after a one-way ANOVA, Tukey's post-hoc test.

appear to increase use and loading of the bone following orthopedic surgery-induced skeletal pain,¹⁶ suggesting that anti-NGF may generally increase the ability of patients to load and use their injured and/or aging skeleton. As loading and use of the skeleton itself has been shown to reduce the expression of sclerostin in bone,^{40,51} anti-sclerostin and anti-NGF may be able to simultaneously build bone and reduce skeletal pain in geriatric patients. If these two therapies do have a synergistic effect, they have the potential to significantly improve the functional status and quality of life of geriatric patients at risk for painful age-related bone fractures.

Author Contributions

PWM conceived and designed this project. Imaging and all analysis was performed by MLT and SRC. All authors contributed to the interpretation of data, writing, review, and/or revision of the manuscript. Additional editing assistance was provided by SAM. Study supervision was led by PWM.

Acknowledgments

We would like to thank Lisa Majuta for her assistance with the animal experiments. In addition, we would also like to thank Drs. Kris Poulsen and David Shelton (Rinat/Pfizer) for kindly providing us the anti-sclerostin sequestering antibody. Dr. Mantyh has served as a consultant and/or received research grants from Abbott (Abbott Park, IL), Adolor (Exton, PA), Array Biopharma (Boulder, CO), Johnson and Johnson (New Brunswick, NJ), Merck (White Plains, New York), Pfizer (New York, NY), Plexxikon (Berkeley, CA), Rinat (South San Francisco, CA), and Roche (Palo Alto, CA).

Declaration of Conflicting Interests

The author(s) declared no potential conflicts of interest with respect to the research, authorship, and/or publication of this article.

Funding

The author(s) disclosed receipt of the following financial support for the research, authorship, and/or publication of this

article: This work was financially supported by NIH Grants CA154550, CA157449, and NS023970 to Patrick Mantyh.

References

1. Exton-Smith AN, Millard PH, Payne PR, et al. Pattern of development and loss of bone with age. *Lancet* 1969; 2: 1154–1157.
2. Firooznia H, Golimbu C, Rafii M, et al. Quantitative computed tomography assessment of spinal trabecular bone. II. In osteoporotic women with and without vertebral fractures. *J Comput Tomogr* 1984; 8: 99–103.
3. Woolf AD and Pfleger B. Burden of major musculoskeletal conditions. *Bull World Health Organ* 2003; 81: 646–656.
4. Melton LJ 3rd. Epidemiology of hip fractures: implications of the exponential increase with age. *Bone* 1996; 18: 121S–125S.
5. Ferguson VL, Ayers RA, Bateman TA, et al. Bone development and age-related bone loss in male C57BL/6J mice. *Bone* 2003; 33: 387–398.
6. Yates LB, Karasik D, Beck TJ, et al. Hip structural geometry in old and old-old age: similarities and differences between men and women. *Bone* 2007; 41: 722–732.
7. Rollman GB and Lautenbacher S. Sex differences in musculoskeletal pain. *Clin J Pain* 2001; 17: 20–24.
8. Gruber R, Koch H, Doll BA, et al. Fracture healing in the elderly patient. *Exp Gerontol* 2006; 41: 1080–1093.
9. Svensson H, Olofsson E, Karlsson J, et al. A painful, never ending story: older women's experiences of living with an osteoporotic vertebral compression fracture. *Osteoporosis Int* 2016; 27: 1729–1736.
10. Mantyh PW. The neurobiology of skeletal pain. *Eur J Neurosci* 2014; 39: 508–519.
11. Roberts SJ, van Gastel N, Carmeliet G, et al. Uncovering the periosteum for skeletal regeneration: the stem cell that lies beneath. *Bone* 2015; 70: 10–18.
12. Alves CJ, Neto E, Sousa DM, et al. Fracture pain-traveling unknown pathways. *Bone* 2016; 85: 107–114.
13. O'Connor JP, Capo JT, Tan V, et al. A comparison of the effects of ibuprofen and rofecoxib on rabbit fibula osteotomy healing. *Acta Orthop* 2009; 80: 597–605.
14. Simon AM and O'Connor JP. Dose and time-dependent effects of cyclooxygenase-2 inhibition on fracture-healing. *J Bone Joint Surg Am* 2007; 89: 500–511.
15. Giannoudis PV, MacDonald DA, Matthews SJ, et al. Nonunion of the femoral diaphysis. The influence of reaming and non-steroidal anti-inflammatory drugs. *J Bone Joint Surg Br* 2000; 82: 655–658.
16. Majuta LA, Longo G, Fealk MN, et al. Orthopedic surgery and bone fracture pain are both significantly attenuated by sustained blockade of nerve growth factor. *Pain* 2015; 156: 157–165.
17. Bala Y, Zebaze R and Seeman E. Role of cortical bone in bone fragility. *Curr Opin Rheumatol* 2015; 27: 406–413.
18. Allen MR, Hock JM and Burr DB. Periosteum: biology, regulation, and response to osteoporosis therapies. *Bone* 2004; 35: 1003–1012.
19. Seeman E. Periosteal bone formation – a neglected determinant of bone strength. *N Engl J Med* 2003; 349: 320–323.
20. O'Driscoll SW, Saris DB, Ito Y, et al. The chondrogenic potential of periosteum decreases with age. *J Orthop Res* 2001; 19: 95–103.
21. Li X, Ominsky MS, Warmington KS, et al. Sclerostin antibody treatment increases bone formation, bone mass, and bone strength in a rat model of postmenopausal osteoporosis. *J Bone Miner Res* 2009; 24: 578–588.
22. Ominsky MS, Vlasseros F, Jolette J, et al. Two doses of sclerostin antibody in cynomolgus monkeys increases bone formation, bone mineral density, and bone strength. *J Bone Miner Res* 2010; 25: 948–959.
23. Tian X, Setterberg RB, Li X, et al. Treatment with a sclerostin antibody increases cancellous bone formation and bone mass regardless of marrow composition in adult female rats. *Bone* 2010; 47: 529–533.
24. Shahnazari M, Wronski T, Chu V, et al. Early response of bone marrow osteoprogenitors to skeletal unloading and sclerostin antibody. *Calcif Tissue Int* 2012; 91: 50–58.
25. Suen PK, Zhu TY, Chow DH, et al. Sclerostin antibody treatment increases bone formation, bone mass, and bone strength of intact bones in adult male rats. *Sci Rep* 2015; 5: 15632.
26. Spatz JM, Ellman R, Cloutier AM, et al. Sclerostin antibody inhibits skeletal deterioration due to reduced mechanical loading. *J Bone Miner Res* 2013; 28: 865–874.
27. Lin C, Jiang X, Dai Z, et al. Sclerostin mediates bone response to mechanical unloading through antagonizing Wnt/beta-catenin signaling. *J Bone Miner Res* 2009; 24: 1651–1661.
28. Moustafa A, Sugiyama T, Prasad J, et al. Mechanical loading-related changes in osteocyte sclerostin expression in mice are more closely associated with the subsequent osteogenic response than the peak strains engendered. *Osteoporosis Int* 2012; 23: 1225–1234.
29. Tian X, Jee WS, Li X, et al. Sclerostin antibody increases bone mass by stimulating bone formation and inhibiting bone resorption in a hindlimb-immobilization rat model. *Bone* 2011; 48: 197–201.
30. Baldauf K and Reymann KG. Influence of EGF/bFGF treatment on proliferation, early neurogenesis and infarct volume after transient focal ischemia. *Brain Res* 2005; 1056: 158–167.
31. Cao JJ, Kurimoto P, Boudignon B, et al. Aging impairs IGF-I receptor activation and induces skeletal resistance to IGF-I. *J Bone Miner Res* 2007; 22: 1271–1279.
32. Soames AR, Lavender D, Foster JR, et al. Image analysis of bromodeoxyuridine (BrdU) staining for measurement of S-phase in rat and mouse liver. *J Histochem Cytochem* 1994; 42: 939–944.
33. Tatematsu M, Mutai M, Aoki T, et al. Proliferation kinetics of pepsinogen altered pyloric gland cells in rats treated with N-methyl-N'-nitro-N-nitrosoguanidine. *Carcinogenesis* 1989; 10: 907–911.
34. Chang H and Knothe Tate ML. Concise review: the periosteum: tapping into a reservoir of clinically useful progenitor cells. *Stem Cells Transl Med* 2012; 1: 480–491.
35. Ochareon P and Herring SW. Cell replication in craniofacial periosteum: appositional vs. resorptive sites. *J Anat* 2011; 218: 285–297.

36. Chartier SR, Thompson ML, Longo G, et al. Exuberant sprouting of sensory and sympathetic nerve fibers in non-healed bone fractures and the generation and maintenance of chronic skeletal pain. *Pain* 2014; 155: 2323–2336.
37. Horner PJ, Power AE, Kempermann G, et al. Proliferation and differentiation of progenitor cells throughout the intact adult rat spinal cord. *J Neurosci* 2000; 20: 2218–2228.
38. Roberts WE, Mozsary PG and Klingler E. Nuclear size as a cell-kinetic marker for osteoblast differentiation. *Am J Anat* 1982; 165: 373–384.
39. Zouani OF, Rami L, Lei Y, et al. Insights into the osteoblast precursor differentiation towards mature osteoblasts induced by continuous BMP-2 signaling. *Biol Open* 2013; 2: 872–881.
40. Thompson ML, Jimenez-Andrade JM and Mantyh PW. Sclerostin immunoreactivity increases in cortical bone osteocytes and decreases in articular cartilage chondrocytes in aging mice. *J Histochem Cytochem* 2016; 64: 179–189.
41. Ke HZ, Richards WG, Li X, et al. Sclerostin and Dickkopf-1 as therapeutic targets in bone diseases. *Endocr Rev* 2012; 33: 747–783.
42. Van Bezooijen R, Bronckers A, Gortzak R, et al. Sclerostin in mineralized matrices and van Buchem disease. *J Dent Res* 2009; 88: 569–574.
43. Brunkow ME, Gardner JC, Van Ness J, et al. Bone dysplasia sclerosteosis results from loss of the SOST gene product, a novel cystine knot-containing protein. *Am J Hum Genet* 2001; 68: 577–589.
44. Balemans W, Patel N, Ebeling M, et al. Identification of a 52 kb deletion downstream of the SOST gene in patients with van Buchem disease. *J Med Genet* 2002; 39: 91–97.
45. Loots GG, Kneissel M, Keller H, et al. Genomic deletion of a long-range bone enhancer misregulates sclerostin in Van Buchem disease. *Genome Res* 2005; 15: 928–935.
46. van Lierop AH, Hamdy NA, Hamersma H, et al. Patients with sclerosteosis and disease carriers: human models of the effect of sclerostin on bone turnover. *J Bone Miner Res* 2011; 26: 2804–2811.
47. Long F. Building strong bones: molecular regulation of the osteoblast lineage. *Nat Rev Mol Cell Biol* 2012; 13: 27–38.
48. Chang DS, Hsu E, Hottinger DG, et al. Anti-nerve growth factor in pain management: current evidence. *J Pain Res* 2016; 9: 373–383.
49. Schnitzer TJ and Marks JA. A systematic review of the efficacy and general safety of antibodies to NGF in the treatment of OA of the hip or knee. *Osteoarthritis Cartilage* 2015; 23: S8–S17.
50. Katz N, Borenstein DG, Birbara C, et al. Efficacy and safety of tanezumab in the treatment of chronic low back pain. *Pain* 2011; 152: 2248–2258.
51. Robling AG, Niziolek PJ, Baldridge LA, et al. Mechanical stimulation of bone in vivo reduces osteocyte expression of Sost/sclerostin. *J Biol Chem* 2008; 283: 5866–5875.